JOURNAL OF MATERIALS SCIENCE **36** (2001) 3079–3087

Single fibre deformation studies of poly(*p*-phenylene benzobisoxazole) fibres

Part I *Determination of Crystal Modulus*

R. J. DAVIES, M. A. MONTES-MORÁN
Manchester Materials Science Centre, UMIST/University of Manchester, Grosvenor St, Manchester M1 7HS, UK

C. RIEKEL
European Synchrotron Radiation Facility, B.P. 220, F-38043, Grenoble Cedex, France

R. J. YOUNG*
Manchester Materials Science Centre, UMIST/University of Manchester, Grosvenor St, Manchester M1 7HS, UK
E-mail: robert.young@umist.ac.uk

This paper constitutes the first part of a study to assess the influence of processing conditions on the final properties of poly(*p*-phenylene benzobisoxazole) PBO fibres. Three different samples were selected: as-spun (AS), high-modulus (HM), and ultra-high modulus (HM+) fibres. Synchrotron radiation was used to obtain single-fibre diffraction patterns. It is the first time this approach is taken to estimate the effects of deformation on the crystal properties of PBO fibres. The crystal modulus of the different types of fibre was calculated from the variation with stress of the *c*-spacing determined from the shift of the (005) and (006) reflections. The HM fibre was found to have the highest crystal modulus of the three fibres, with AS and HM+ PBO being lower. In comparison with tensile data, none of the fibres were found to have a Young's modulus near to the crystal modulus value, although the HM+ fibre was closest due to its production route. These results could be compared to previous diffraction experiments, where the crystal modulus of PBO fibres were determined using fibre-bundles, assuming homogeneous stress in the bundle. Also, Raman spectroscopy experiments were carried out to examine the differences in Raman bandshift rates in response to both stress and strain. The Raman results showed both the HM and HM+ fibres to have stress-induced bandshifts of approximately $-4\,cm^{-1}$/GPa. The AS fibre value was significantly lower, this being attributed to the non-uniformity of the fibre cross-section. The strain-induced Raman bandshifts were found to be dependent on the tensile modulus of the fibre.

1. Introduction

Poly(*p*-phenylene benzobisoxazole) or PBO fibres are aromatic rigid-rod polymeric fibres which demonstrate remarkably high modulus and strength values, far in excess of almost all other so-called 'high-performance' polymeric fibres [1]. The chemical structure of the PBO molecule is as follows.

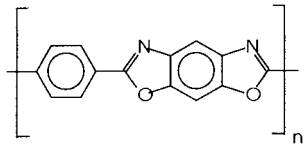

The development of PBO fibres has progressed over three decades from the initial concept during the US Air Force's Ordered Polymer programme until their recent commercialisation by Toyobo (Japan) as the fibre 'Zylon^{TM}'. These fibres have excellent axial chain orientation and a highly crystalline structure, making them ideal subjects for experimental techniques such as Raman spectroscopy and X-ray diffraction (XRD). The crystal structure of PBO was first determined successfully in 1980 by Choe *et al*. [2] although there have been several revisions made to the model in the intervening years [3, 4, 5]. The unit cell of PBO has been shown to have a non-primitive monoclinic structure [3].

At present, PBO fibres are produced in two varieties, as-spun (AS) and high-modulus (HM). The production of both of these is thought to involve a dry-jet wet spinning process from air into an aqueous solution. Whilst the AS fibre is commercialised literally 'as-spun', the HM fibre is given a subsequent heat treatment process

* Author to whom all correspondence should be addressed.

which is responsible for improving the Young's modulus of the fibre. A third fibre, HM+, is currently being developed which is produced using a revised non-aqueous spinning method. Kitagawa *et al*. [6] have shown it to have a Young's modulus far greater than that of HM, and have attributed this to the reduction in density fluctuations resulting from the different spinning conditions. It has been proposed that these fluctuations are the reason why the theoretical modulus of the PBO fibres (i.e. that calculated crystallographically) is not similar to that measured experimentally in tensile testing [6]. It therefore follows that by reducing these fluctuations, the Young's modulus can be increased towards its theoretical value.

This paper constitutes the first in a series that will examine single-fibre deformation of PBO fibres using a combination of synchrotron XRD studies, tensile testing and Raman spectroscopy. From analysis of all three PBO fibre varieties (AS, HM and HM+), conclusions can be drawn as to the influence of processing differences on the properties of the fibres produced. This first paper of the series is concerned primarily with determination and comparison of single-fibre crystal modulus values for three varieties of PBO, with future papers examining other elements from the diffraction patterns such as local crystallite orientation.

Previous diffraction experiments on PBO AS and HM have enabled their crystal modulus values to be calculated from meridional x-ray diffractograms using a method based loosely on theory proposed by Dulmage and Contois in 1958 [7]. Lenhert and Adams [8] were the first to complete successfully such an experiment for PBO using fibre bundles in 1989, although more recently other research groups have replicated their results [6]. The measured crystal modulus values have also been found to be close to a theoretical modulus calculated using lattice-dynamical equations by Tashiro and Kobayashi [9]. Although the crystal modulus values of PBO AS and HM have been examined in some depth by various research groups, the crystal modulus of PBO HM+ has yet to be published.

To date, the crystal modulus of PBO fibre has still to be determined from single-fibre diffraction patterns, although this has been performed for aramid fibres using synchrotron radiation by Riekel *et al*. [10]. By using this method, rather than the fibre bundle technique, the validity of employing a homogeneous stress assumption (i.e. the load on the crystals is the applied load divided by the cross sectional area of the fibres) can be investigated. This issue has been discussed before in assessing experimental accuracy when determining particular fibre properties, such as the account given by Holliday and White [11]. Although the similarities between the calculated theoretical modulus of PBO fibres [9] and their measured crystal modulus [6], with the additional single-fibre results shown from aramids [10], would indicate that such an assumption holds true for crystal modulus calculations, analysis of the validity of this assumption for PBO is only possible with calculations from single-fibre diffraction patterns, such as those generated with synchrotron radiation.

The synchrotron XRD study of PBO AS, HM and HM+ has enabled the crystal modulus of the fibres to be calculated using the meridional reflections generated from single-fibre diffraction patterns. This allows a direct comparison of the three PBO fibre varieties, and combined with the use of other experimental methods, a comprehensive account of differences in the AS, HM and HM+ fibres response to deformation can be generated. For example, the tensile testing of PBO samples allows an indication of the actual tensile properties achieved by the fibres, rather than their theoretical properties. As previously mentioned, this can then be used when assessing the reduction in tensile properties due to processing conditions, as shown in the density fluctuation observations for HM+ [6].

Raman spectroscopy can also be used to examine deformation of the PBO molecule, as was originally performed by Mitra and Risen on polydiacetylene single crystal fibres in 1977 [12]. Previous studies have shown that PBO produces particularly well defined spectra in comparison to other materials due to its highly crystalline structure [13], as also found with PBT [14]. Of the five principal Raman bands from the PBO spectrum, it is known that several are sensitive to induced stress or strain [15, 16]. Furthermore, previous studies of the 1618 cm^{-1} Raman band for PBO have shown that strain-induced band shift depends on the Young's modulus of the fibre [15, 16]. Similarly, the stress-induced band shift has been found to remain at -4 cm^{-1}/GPa regardless of fibre properties [16]; the same value as has been found with other aromatic main-chain polymers [17]. Although not fully understood, this is significant as it indicates that similar deformation characteristics can be found in materials that are chemically dissimilar.

2. Experimental

2.1. Materials

Three different types of PBO fibre, namely AS, HM and HM+ were characterised. The AS (as spun) and HM (high modulus) fibres are produced commercially by Toyobo (Zylon®). The PBO HM+ fibre is currently still in the development stage, although it is known that it was produced using a non-aqueous coagulation process, further details of which can be found elsewhere [6].

2.2. Scanning Electron Microscopy (SEM)

A Philips series XL-30 Field Emission Gun Scanning Electron Microscope (FEG-SEM) was used to determine accurately the diameter of the fibres used in this work. The diameter measurements were made using three different levels of magnification, all of which had been previously calibrated using a graticule. At least ten fibres were then selected at random for each variety of PBO and the average and standard deviation calculated for each.

2.3. Tensile testing

Tensile testing of the single-fibre specimens was carried out using an Instron 1121 universal testing machine using a 1 N load cell and Workbench data logging software. All testing was carried out in a standard

atmosphere at a cross-head speed of 2 mm min^{-1}, using samples that had been pre-conditioned for a minimum of 24 hours. The samples were prepared within cardboard windows, and fixed in place using cold-curing epoxy resin.

Previous studies have shown that both Young's modulus and tensile strength are gauge length sensitive [18, 19]. As a result, testing of each variety of PBO was undertaken using 3 different gauge lengths, 20 mm, 50 mm and 100 mm using at least ten samples at each length. The modulus results were then extrapolated to infinite gauge length in order to eliminate the influence of end effects, and strength results extrapolated to zero gauge length to account for the influence of critical flaws.

2.4. Raman spectroscopy

Raman spectroscopy was carried out on all three samples using a Renishaw System 1000 Spectrometer, with a He-Ne laser. The beam was focused onto the surface of the specimen at a diameter of 2-3 μm using the $\times 50$ magnification lens of an Olympus BH-2 microscope. The back-scattered light was detected using a Renishaw charge-coupled device (CCD) camera, and the data processed using Renishaw Grams/32® software version 4.14. All samples were prepared using cardboard windows at a gauge length of 50 mm, and fixed using cold-curing epoxy resin.

Two types of Raman scan were performed on the samples, the first was an extended scan to examine the entire Raman spectrum, with the second being a static scan in order to examine Raman band shift rates with deformation. The extended scans were performed from 800 cm^{-1} to 1800 cm^{-1}, so that all first-order Raman bands for each variety of PBO could be detected. Each scan took 30 s, and the background fluorescence from the resulting data was deducted to improve clarity of the plots.

Deformation studies were performed with the use of a single-fibre stretching rig. The rig consists of a 2 N load cell to which one end of the fibre was connected, and a micrometer at the other. By applying a known extension to the fibre using the micrometer, the corresponding load was measured using a transducer indicator connected to the load cell, and Raman data captured simultaneously. Graphs were then constructed showing the change in Raman wavenumber for a particular Raman band of PBO against stress and strain. The Raman scans took 2 s, and only a selected area of the spectrum close to the 1618 cm^{-1} Raman band was recorded. This band was chosen, as it is known to shift significantly with fibre deformation [20].

2.5. X-ray diffraction (XRD)

XRD characterisation of the fibres was carried out at the European Synchrotron Radiation Facility (ESRF) on beamline ID13 (micro-focus beamline). The beamline was configured with the beam stopped down to a 3 μm diameter spot size and a MARCCD detector. The specimen-to-film distance was calculated using an Al_2O_3 sample and was found to be approximately 68 mm. The fibres were loaded using a single-fibre stretching rig that was designed to fit to the x-y-z drive plate of the beamline stage. The deformation rig is based on a piezo stretching mechanism, and the load measured using an incorporated load cell. The gauge length between the mounting plates of the rig was 3.8 mm with a full deflection of 280 μm. Samples were glued (cyanoacrylate adhesive) directly to the mounting plates, and cured in-situ prior to collection of data. Both the piezo mechanism and the recording of the load cell data were monitored from within the control cabin. A diffraction pattern (15 s of scan time) was taken from the centre of the fibre sample at increasing levels of loading, until either fibre fracture or de-bonding from the adhesive took place. This procedure was performed for all three PBO fibres.

Analysis of the results was carried out using the Fit2d software application version 10.95 [21, 22]. In order to calculate the crystal modulus, it was first necessary to determine the position of the meridional reflections from beam centre. This was achieved using caking functions, which allow the integration of intensity data in the radial direction (Fig. 1a). From the integrated data, Voigtian peaks were fitted to determine the precise peak position as shown in Fig. 1b.

In order to increase the accuracy of the result, both (005) and (006) reflections were used to calculate c-spacing. These peaks were chosen as they showed the best definition and were therefore easiest to fit. Due to constant corrections that were required in order to maintain the beam alignment, small changes in the beam centre position could occur. To overcome this, (005) and (006) reflections both above and below the beam centre were used to extract peak position, and then an average was taken. In this way, any small vertical changes in beam position would be cancelled out.

Once the peak positions were determined at all load levels, 1-dimensional diffraction grating theory was used in order to calculate c-spacing [23], shown in Equation 1:

$$c = \frac{n\lambda}{\sin\left(\tan^{-1}\left(\frac{x}{r}\right)\right)} \quad (1)$$

where n is the reflection index, λ the radiation wavelength, x the reflection vertical height and r the specimen-to-film distance. By taking the change in c-spacing as the strain in the stress/strain graph and assuming uniform stress within the fibres, the crystal modulus can be extracted as the gradient.

3. Results and discussion

3.1. Fibre morphology

Fig. 2 shows SEM micrographs of PBO HM fibres. These images are also representative of the AS and HM+ fibres, thus suggesting that both the heat treatment and alternative coagulation method have no visible effect on the fibre surface. The fibres are essentially circular in cross section, with a smooth, regular surface, as shown in Fig. 2a. Diameters of all three fibres

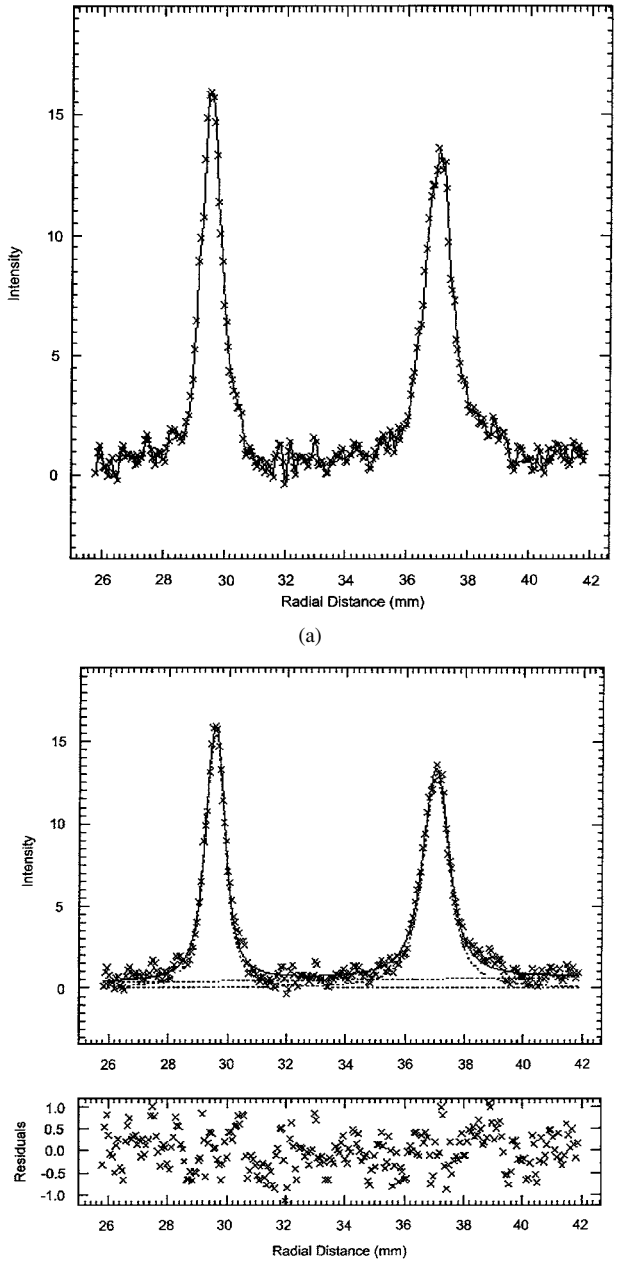

(a)

(b)

Figure 1 Curve fitting for the (005) and (006) Bragg peaks. a) Cake segment integrated azimuthally for the (005) and (006) reflections b) Fitted (005) and (006) reflections showing residuals.

were measured from random samples of up to ten single fibres, and the results are collected in Table I. Relatively high standard deviations ($\sim\pm1$ μm, Table I) were obtained for all three types of fibre, which reveals that it is the spinning process that results in the large fluctuations in the diameters of the fibre produced, rather than subsequent heat-stretching treatments, as has been reported previously [24]. On the other hand, differences in diameter between the AS type of fibre and both HM and HM+ are significant. This indicates that the treatments carried out to improve the mechanical properties of the fibre lead to a reduction of its diameter.

TABLE I Dimensions and mechanical properties of the PBO fibres studied

	Fibre Diameter (μm)	Strength (GPa)	Modulus (GPa)
AS	12.3 (±1.1)	4.8 (±0.6)	180 (±10)
HM	11.2 (±1.0)	5.5 (±0.7)	254 (±19)
HM+	11.6 (±1.2)	5.4 (±0.9)	330 (±30)

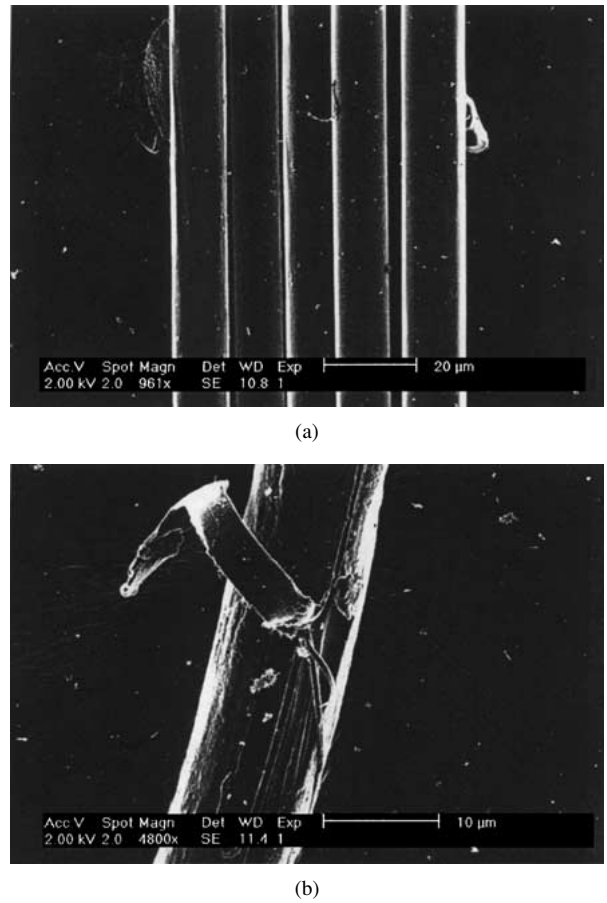

(a)

(b)

Figure 2 FEG-SEM Micrographs of PBO fibres. a) Several parallel PBO fibres. b) A single damaged PBO fibre showing the inner fibrillar structure.

The existence of a fibrillar structure of PBO and other high performance fibres has been reported previously [6, 24, 25, 26]. Fig. 2b shows a section of a delaminated fibre surface, where the internal fibrils of dimensions $\sim$0.5 μm can be discerned. These fibrils consist of highly oriented PBO chains parallel to the fibre (c-) axis, with the a-axes of the crystals aligned radially across the fibre [26].

3.2. Tensile testing

Fig. 3 shows typical stress-strain curves for the three PBO samples under study, at 50 mm gauge length. It can be seen that the deformation is approximately linear up to fracture, with occurrence of slight initial strain hardening. The tensile strength and Young's modulus, extrapolated to infinite and zero gauge length respectively (see Experimental section), of the three types of fibre are shown in Table I. The tensile strength values of the AS, HM and HM+ fibres are similar, with any observed difference being within the error values.

The tensile modulus values shown in Table I agree well with those reported in a recent article of Kitagawa *et al*. [6]. The AS fibre displays a considerably lower

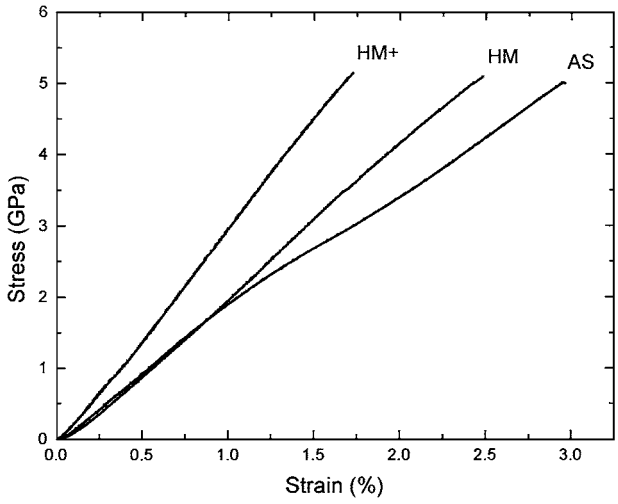

Figure 3 Tensile stress/strain curves for PBO AS, HM and HM+ fibres.

Young's modulus compared to those of the HM and HM+ fibres. This can be attributed to the heat treatments in the HM and HM+ processing route, which are designed specifically to impart improved tensile properties to the fibres. Additionally, there is a significant difference in the Young's modulus of the HM and HM+ fibres where the HM+ fibre modulus is ∼60 GPa greater than that of the HM fibre. This difference has been previously documented [6] and can be attributed to the different processing routes of the two fibres. It is thought that the non-aqueous coagulation process which is used in the production of the HM+ fibre results in fewer periodic density fluctuations, resulting in a tensile modulus nearer to that predicted theoretically [6].

3.3. Raman spectroscopy

Fig. 4 shows the Raman spectra of the three types of PBO fibre under study, in the range of 800 to 1800 cm^{-1}. Several prominent Raman bands can be observed, the 1618 cm^{-1} feature being the most intense. This band has been attributed to the stretching of the *p*-phenylene ring. No significant differences arise when the spectra of the three types of fibre are compared. Clearly, however, the definition of the Raman spectrum increases as the modulus of the fibre decreases. This could be explained by attributing the reduction in clarity to the heat treatment processing of the HM and HM+ fibres. Apart from the possible concentration of solvent in the outer layers of the HM+ fibre, the eventual chemical modification of the fibre skin due to the relatively high temperatures reached during the final step of the processing could bring about the strong fluorescence background observed in the HM and HM+ Raman spectra.

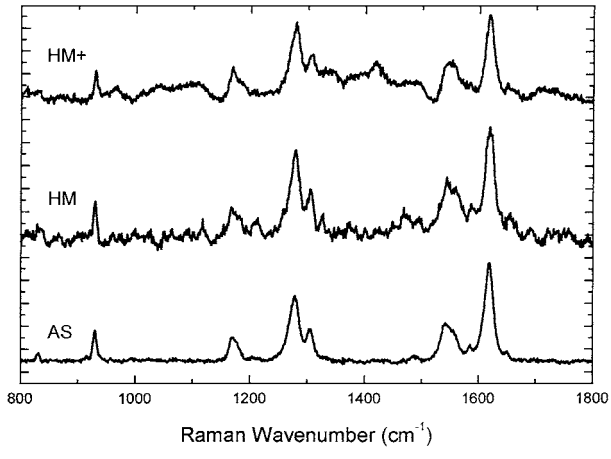

Figure 4 Extended Raman spectra for PBO AS, HM and HM+ fibres in the range 800–1800 cm^{-1}.

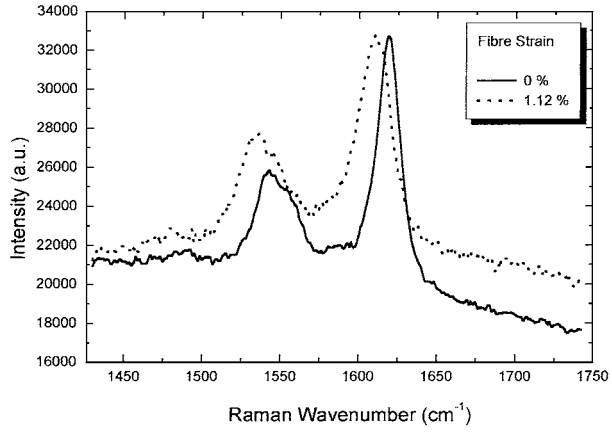

Figure 5 Example of the Raman band shift with strain for a PBO HM fibre.

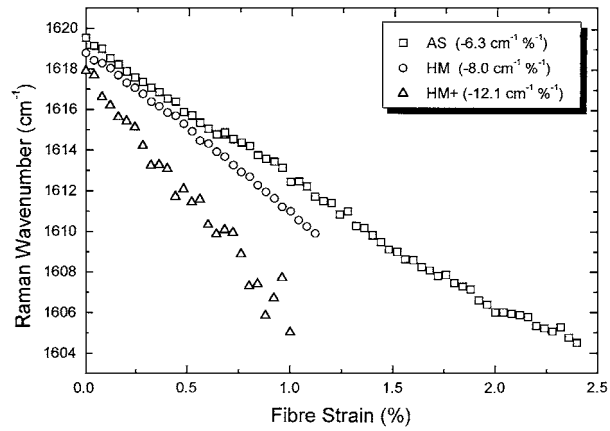

Figure 6 Dependence of the peak positions of the 1618 cm^{-1} Raman band with strain for the PBO AS, HM and HM+ fibres.

It is well known that certain Raman bands shift upon the application of stress (or strain) on the fibre [15, 16]. Fig. 5 shows the shifts of the 1540 cm^{-1} and 1618 cm^{-1} Raman bands of a PBO HM filament as a response to external strain. It can be observed that the peak position shifts to a lower wavenumber when the fibre is under tension and a broadening of the Raman band can also be noticed. The variation of the 1618 cm^{-1} Raman band position with tensile strain is shown in Fig. 6, where an approximately linear shift can be observed for all types of fibre. Table II shows the rate of band shift per unit stress and strain (or stress and strain sensitivity factors, respectively) corresponding to the three fibre types. It can be seen that the stress induced band shift rates for PBO HM and HM+ agree favourably with the −4 cm^{-1}/GPa band shift rate that has been found for other aromatic high-modulus fibres [17]. The AS fibre has a lower band shift rate, however, due possibly to

TABLE II Stress- and strain-induced shift data for the 1618 cm^{-1} Raman band along with derived modulus values

	Strain-induced Bandshift (cm^{-1}/%)	Stress-induced Bandshift (cm^{-1}/GPa)	Young's Modulus* (GPa)	
			Spectroscopic	Mechanical
AS	−6.3 (±0.4)	−3.3 (±0.3)	190	170
HM	−8.0 (±0.3)	−3.5 (±0.4)	230	240
HM+	−12.1 (±1.4)	−4.3 (±0.3)	280	300

*(50 mm gauge length)

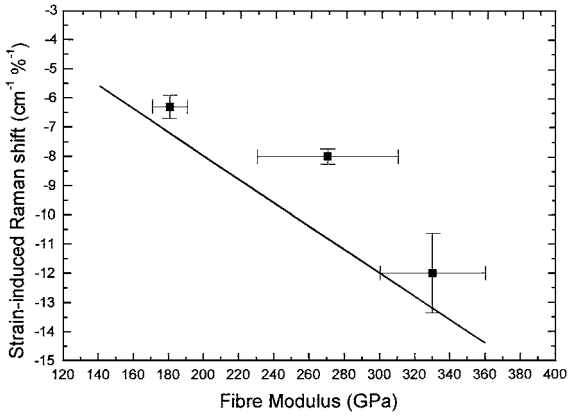

Figure 7 Dependence of the strain-induced Raman band shift upon fibre tensile modulus for the PBO AS, HM and HM+ fibres. (The solid line is from the work of Yeh and Young [20] upon aromatic polymer fibres).

large differences between the skin and core structure of the fibre, as has been observed in previous studies on aramid fibres [15]. Since Raman spectroscopy is a surface characterisation technique, any variations in uniformity from fibre surface to core need to be taken into consideration.

The strain-induced Raman band shift rates agree favourably with those obtained from previous studies [16]. The relationship between Young's modulus and band shift rate is evident, with the HM+ fibre having the highest rate, followed by the HM fibre, then the AS fibre (Fig. 7). This phenomenon has been observed in many rigid-rod polymers [15, 16]. Yeh and Young [20] have published recently a Raman study of several aromatic main chain polymers (PET, aramids and PBO). They found a linear dependence of the Raman band shift rate corresponding to the aromatic rings with the fibre tensile modulus. This *universal* relationship shown as a continuous line in Fig. 7 seems to agree well with the results presented in the present work.

The so-called "spectroscopic" Young's modulus can be calculated from both stress and strain sensitivity factors [20]. These results are also collected in Table II, and, in general, agree well with the Young's moduli measured by conventional tensile tests at 50 mm gauge length (Table II).

3.4. Synchrotron XRD studies

Fig. 8 shows the unloaded (top) and loaded (bottom) single-fibre diffraction patterns of PBO AS, HM and HM+ collected at the ESRF. From these diffraction patterns, several features can be observed. The strong

TABLE III FWHM data for the XRD Bragg reflections and Raman bands for the PBO fibres

	XRD Reflections (mm)		1618 cm^{-1} Raman Band (cm^{-1})
	(005)	(006)	
AS	1.07	1.77	18.3 (±0.2)
HM	0.75	1.04	18.7 (±0.8)
HM+	0.59	0.87	18.2 (±1.2)

equatorial reflections and multiple meridional reflections indicate a high degree of crystallite orientation along the fibre axis and suggest a good lateral packing of the stiff-molecules within the fibre, for all types of fibre. The presence of off-axis first-order reflections indicates a high degree of three-dimensional crystallinity in all three fibres, although clearly this is greater in the HM+. This superior crystallinity of the HM+ with respect to the rest of the varieties is also reflected in the FWHM (full width at half maximum height), of the meridional reflections, as shown in Table III. For the two main reflections, i.e. (005) and (006), the AS fibre exhibits wider peaks, followed by HM and, finally, PBO HM+ with narrower reflections (typical uncertainties of FWHM measurements being ±0.05 mm). This indicates that the distribution of *c*-spacing in the AS fibre is greater than that of the HM and HM+ varieties. In general terms, it can be seen from the diffraction patterns generated by the three fibre types that the PBO HM+ fibre has a greater clarity and better definition than the HM diffraction pattern, which in turn is superior to that of the AS fibre. This situation differs from the findings obtained by Raman spectroscopy, where (as mentioned in the previous section), the Raman bands are better defined in the case of the AS fibre. The FWHM of the 1618 and 1540 cm^{-1} Raman bands of the three types of fibre are also collected in Table III. In contrast to the XRD observation, the widths of the Raman bands are similar, within experimental error, for all the fibres characterised in this work.

The lower three images of Fig. 8 show the diffraction patterns of the same fibres when subjected to a load. When compared with the unloaded diffraction patterns (Fig. 8 top), streaking of the meridional layer lines can be observed which suggests a decrease in translational disorder of the crystallites in the fibre axis. Of particular interest in comparison of the loaded and unloaded diffraction patterns is the difference in definition of the equatorial peaks before and after loading of the fibres. This indicates the orientation distribution of the crystallites within the fibre improves during loading, a subject that will be discussed in the next paper in this series.

Macroscopic deformation of the fibres will induce changes at microscopic level, specifically interatomic distances, and hence lead to the deformation of the unit cell. Due to the microstructure of the PBO fibres, major changes in atomic distances of the polymer backbone are expected, since the polymeric chains align into microfibrils along the fibre axis (see Section 3.1.). This effect brings about a shift of the meridional reflections with external stress (Fig. 9), analogous to the band shift observed during the Raman spectroscopy experiments

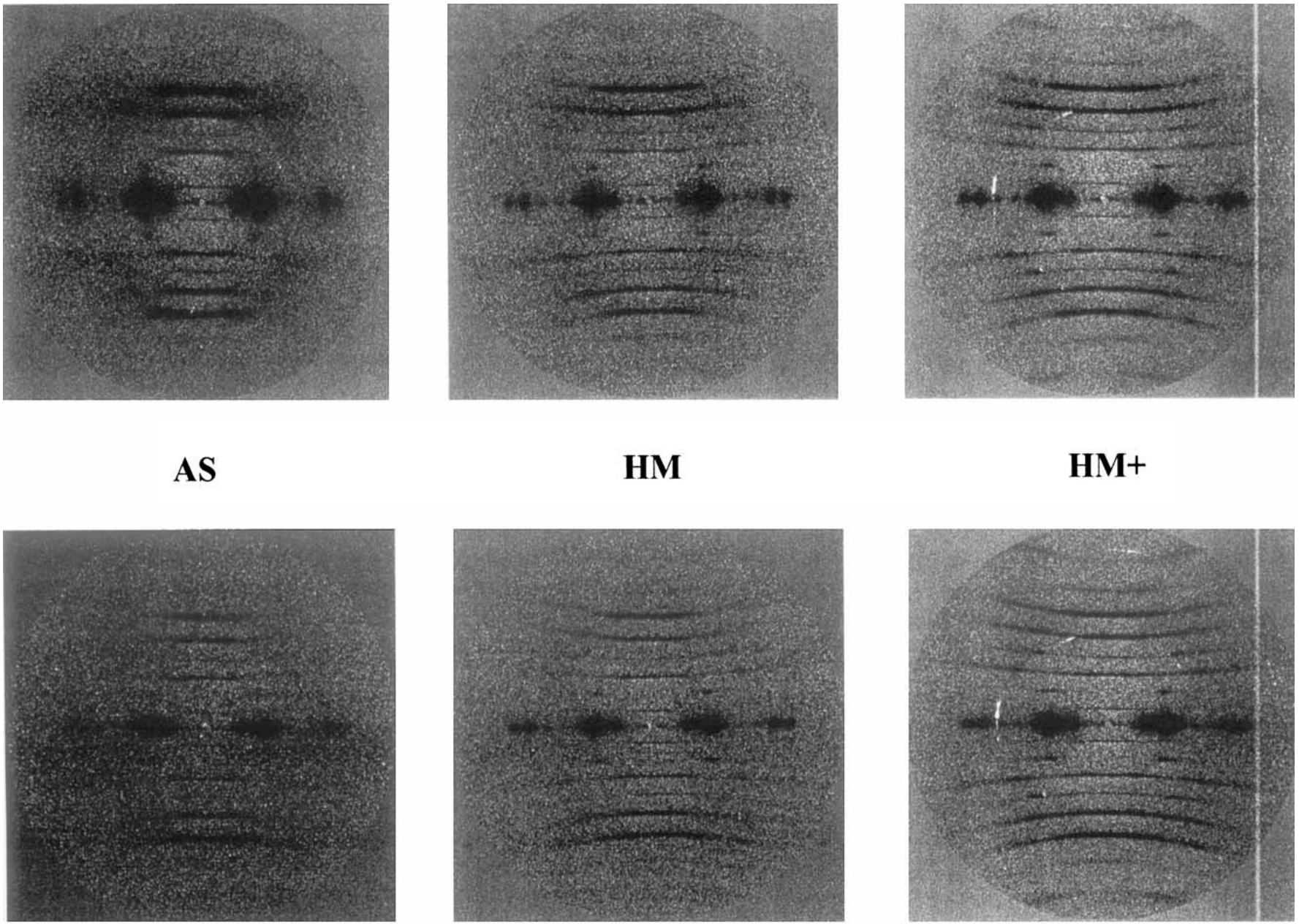

Figure 8 Single-fibre diffraction patterns for unloaded (top row) and loaded (bottom row) PBO AS, HM and HM+ fibres generated using Synchrotron radiation.

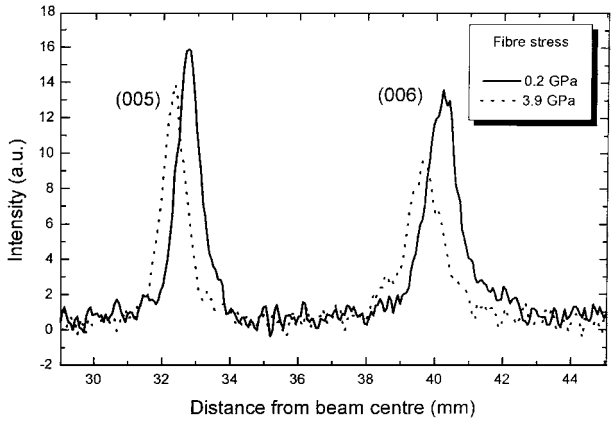

Figure 9 Shift of the (005) and (006) Bragg reflections with stress for a PBO HM fibre.

(Fig. 5). Conversely, however, the mentioned shift of the meridional reflections with stress encompasses a narrowing of the peaks (Fig. 9), whereas broadening is clearly observed for the Raman bands [20] after the deformation of the fibre (Fig. 5).

By measuring the amount of meridional peak movement during the loading of the fibre (Fig. 9), the change in c-spacing (i.e., in the direction of the fibre axis) of the unit cell can be calculated. A microscopic fibre strain can be thus estimated and used finally to determine crystal modulus. Fig. 10 shows the stress versus crystal strain plots and crystal modulus values for each of the three fibre types.

A direct comparison of the three values shows the HM fibre appears to have a crystal modulus significantly higher than that of both the AS and HM+ fibres. This may not be the case as the error tolerance quoted for the crystal modulus value is due to experimental error only, and the influence of fibre diameter variations have not been included. Such variations as those shown in Table I, could result in a systematic error greater than the experimental error, approximately 10% for all three fibre types. This, when combined with the experimental error, results in a total error which would suggest the aforementioned differences in crystal modulus between the fibre types may not exist. This would appear more plausible since all three fibre types are based on the same crystal structure and should therefore have similar crystal modulus values. The influence of diameter on single-fibre diffraction pattern experiments remains the primary obstacle in experimental accuracy. Although such influences are almost eliminated by the use of fibre-bundles, careful experimental practice such as fibre diameter measurements locally to experimental sites can greatly reduce these errors.

In the case of PBO AS and HM, the crystal modulus results generated from single fibre diffraction patterns agree favourably with those previously published using fibre-bundle diffraction [8, 9]. This would therefore indicate that the assumption required for fibre-bundle determination of crystal modulus of homogeneous stress is valid. The result for PBO HM+ cannot be compared with such data, as this is the first time, to our knowledge, that the crystal modulus of this type of PBO fibre has been reported.

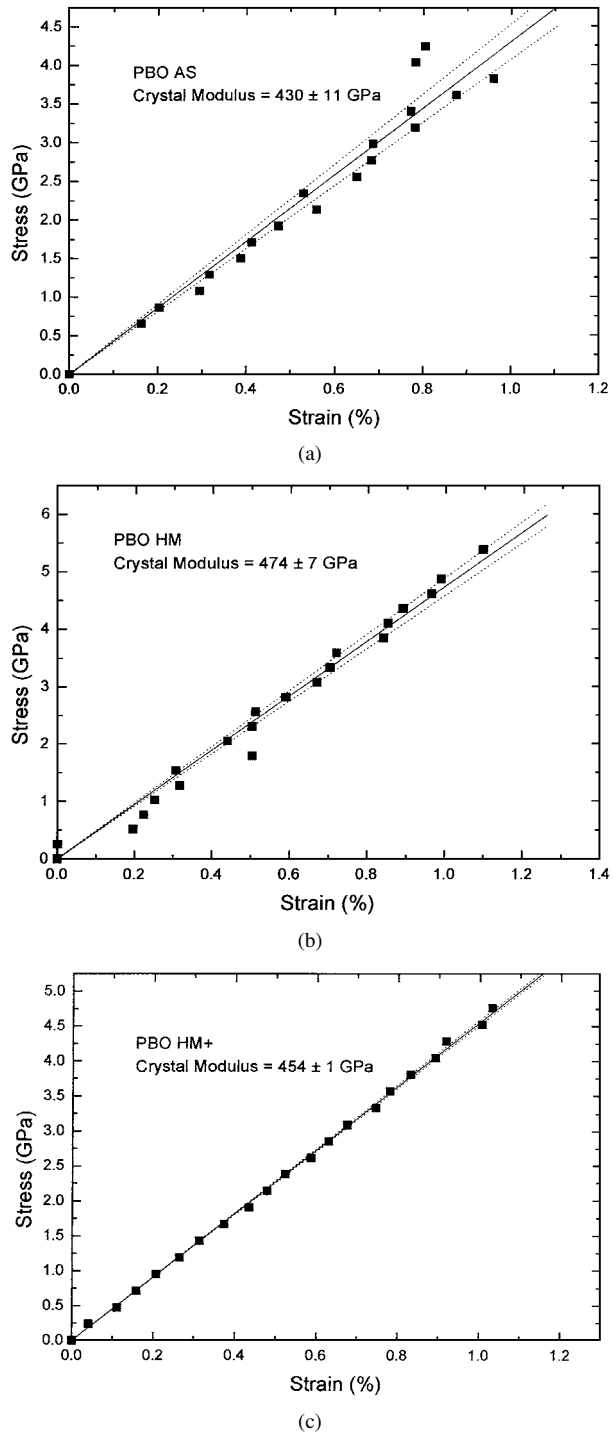

Figure 10 Plots of stress versus crystal strain for single PBO fibres. (The crystal modulus is indicated. The dotted lines are 95% confidence limits). a) Data for a PBO AS fibre. b) Data for a PBO HM fibre. c) Data for a PBO HM+ fibre.

In comparison with the Young's modulus determined from tensile results, it can be seen that all three fibres show a much lower Young's modulus compared to their crystal modulus values. This demonstrates the effect of flaws, impurities, voids and imperfect crystallite orientation within the fibres, all of which lower the measured Young's modulus from its crystal modulus value. Of the three fibre varieties, the HM+ fibre has a Young's modulus much closer to the crystal modulus than the other two types of fibre, the crystal modulus being only 37% greater than the Young's modulus compared to 86% for the HM fibre. This improvement in Young's

modulus can be attributed to the non-aqueous coagulation method used to produce HM+, which is designed to reduce periodic density fluctuations in the fibre. The reduction in such fluctuations has been previously measured using SAXS [6].

4. Conclusions

Raman analysis of the PBO fibres showed that the stress induced bandshift rates for the HM and HM+ fibres were comparable to those for other aromatic high modulus fibres. This was not the case for the AS fibre, although it has been suggested previously that this may be attributed to a non-uniformity between the skin and core of the sample. For the strain induced bandshift rates, the previously documented relationship with tensile modulus was evident, with the HM+ fibre showing the largest band shift rate followed by the HM and AS fibres.

The crystal modulus of PBO HM is greater than that of either PBO AS or PBO HM+ although the reason behind this is not clear. In comparison with tensile data, the crystal modulus of the three fibre types was found to be greater than the Young's modulus. This indicates the influence of factors reducing the measured tensile modulus of the fibres, such as flaws, voids, impurities and poor crystallite orientation. This difference was reduced significantly in the HM+ fibre, which suggests that the non-aqueous coagulation process reduces those factors.

Finally, it can be concluded that the assumption of homogeneous stress when calculating PBO crystal modulus in fibre bundle x-ray diffraction studies is valid, since the same values can be determined from single-fibre diffraction patterns.

Acknowledgements

We would like to extend our thanks to EPSRC for funding this project, the ESRF for beam time, and Toyobo (Japan) for supplying the fibre samples. We would also like to thank Andrew Hammersley for allowing us to use the Fit2D software application. We would also like to acknowledge the help of colleagues at the Manchester Materials Science Centre, in particular Ian Brough for use of the FEG-SEM, and Craig Meakin. One of the authors (M. A. M.-M.) is grateful to MEC (Spain) for a personal grant.

References

1. S. KUMAR, in "Encyclopedia of Composites" (VCH Publishers, NY, 1990) Vol. 14, p. 51.
2. E. W. CHOE and S. N. KIM, *Macromolecules* **14** (1981) 921.
3. A. V. FRATINI, P. G. LENHERT and T. J. RESCH, *Mat. Res. Soc. Symp. Proc.* **134** (1989) 431.
4. D. C. MARTIN and E. L. THOMAS, *Macromolecules* **24** (1991) 2450.
5. K. TASHIRO, J. YOSHINO, T. KITAGAWA, H. MURASE and K. YABUKI, *ibid.* **31** (1998) 5430.
6. T. KITAGAWA, M. ISHITOBI and K. YABUKI, *J. Polym. Sci.* **38** (2000) 1605.
7. W. J. DUMAGE and L. E. CONTOIS, *ibid.* **28** (1958) 275.
8. P. G. LENHERT and W. W. ADAMS, *Mat. Res. Soc. Symp. Proc.* **134** (1989) 329.
9. K. TASHIRO and M. KOBAYASHI, *Macromolecules* **24** (1991) 3706.
10. C. RIEKEL, T. DIEING, P. ENGSTROM, L. VINCZE, C. MARTIN and A. MAHENDRASINGAM, *ibid.* **32** (1999) 7859.
11. L. HOLLIDAY and J. W. WHITE, *Pure and Appl. Chem.* **26** (1971) 545.
12. V. K. MITRA and W. M. RISEN, *J. Chem. Phys.* **66** (1977) 2731.
13. C. L. SO, PhD Thesis, UMIST, UK, 2000.
14. R. J. DAY, I. M. ROBINSON, M. ZAKIKHANI and R. J. YOUNG, *Polymer* **28** (1987) 1833.
15. R. J. YOUNG, R. J. DAY and M. ZAKIKHANI, *J. Mater. Sci.* **25** (1990) 127.
16. T. KITAGAWA, K. YABUKI and R. J. YOUNG, *Polymer* **42** (2001) 2101.
17. R. J. YOUNG, *J. Text. Inst.* **86** (1995) 360.
18. J. IM, P. A. PERCHA and D. S. YEAKLE, *Mat. Res. Soc. Symp. Proc.* **134** (1989) 307.
19. R. J. YOUNG and P. P. ANG, *Polymer* **33** (1992) 975.
20. W.-Y. YEH and R. J. YOUNG, *ibid.* **40** (1999) 857.
21. A. P. HAMMERSLEY, *ESRF Internal Report*, **ESRF97HA02T**, 'FIT2D: an introduction and overview' (1997).
22. A. P. HAMMERSLEY and C. RIEKEL, *Syn. Rad. News* **2** (1989) 24.
23. R. J. YOUNG and P. A. LOVELL, in *Introduction to Polymers Second Edition* (Chapman & Hall, 1991) 243.
24. M. E. HUNSAKER, G. E. PRICE and S. J. BAI, *Polymer* **33** (1992) 2128.
25. S. J. KRAUSE, T. B. HADDOCK, D. L. VERZIE, P. G. LENHERT, W. F. HWANG, G. E. PRICE, T. E. HELMINIAK, J. F. O'BRIEN and W. W. ADAMS, *ibid.* **29** (1988) 1354.
26. T. KITAGAWA, H. MURASE and K. YABUKI, *J. Polym. Sci.* **36** (1998) 39.

Received 18 October
and accepted 23 November 2000